Spin transfer torque generated magnetic droplet solitons (invited)

S. Chung, S. M. Mohseni, S. R. Sani, E. Iacocca, R. K. Dumas, T. N. Anh Nguyen, Ye. Pogoryelov, P. K. Muduli, A. Eklund, M. Hoefer, and J. Åkerman

Citation: Journal of Applied Physics **115**, 172612 (2014); doi: 10.1063/1.4870696
View online: http://dx.doi.org/10.1063/1.4870696
View Table of Contents: http://scitation.aip.org/content/aip/journal/jap/115/17?ver=pdfcov
Published by the AIP Publishing

Spin transfer torque generated magnetic droplet solitons (invited)

S. Chung,[1,2] S. M. Mohseni,[1,3,4] S. R. Sani,[1,3] E. Iacocca,[2] R. K. Dumas,[2] T. N. Anh Nguyen,[1,5] Ye. Pogoryelov,[2] P. K. Muduli,[2,6] A. Eklund,[7] M. Hoefer,[8] and J. Åkerman[1,2,3,a)]

[1]*Materials Physics, School of ICT, Royal Institute of Technology, Electrum 229, 164 40 Kista, Sweden*
[2]*Department of Physics, University of Gothenburg, 412 96 Gothenburg, Sweden*
[3]*NanOsc AB, Electrum 205, 164 40 Kista, Sweden*
[4]*Department of Physics, Shahid Beheshti University, G.C., Evin, Tehran 19839, Iran*
[5]*Laboratory for Nanotechnology (LNT), Vietnam National University - Ho Chi Minh City (VNU-HCM), Ho Chi Minh City, Vietnam*
[6]*Department of Physics, Indian Institute of Technology Delhi, New Delhi 110016, India*
[7]*Devices and Circuits, School of ICT, KTH Royal Institute of Technology, Electrum 229, 164 40 Kista, Sweden*
[8]*Department of Mathematics, North Carolina State University, Raleigh, North Carolina 27695, USA*

(Presented 6 November 2013; received 23 September 2013; accepted 24 October 2013; published online 16 April 2014)

We present recent experimental and numerical advancements in the understanding of spin transfer torque generated magnetic droplet solitons. The experimental work focuses on nano-contact spin torque oscillators (NC-STOs) based on orthogonal (pseudo) spin valves where the Co fixed layer has an easy-plane anisotropy, and the [Co/Ni] free layer has a strong perpendicular magnetic anisotropy. The NC-STO resistance and microwave signal generation are measured simultaneously as a function of drive current and applied perpendicular magnetic field. Both exhibit dramatic transitions at a certain current dependent critical field value, where the microwave frequency drops 10 GHz, modulation sidebands appear, and the resistance exhibits a jump, while the magnetoresistance changes sign. We interpret these observations as the nucleation of a magnetic droplet soliton with a large fraction of its magnetization processing with an angle greater than 90°, i.e., around a direction opposite that of the applied field. This interpretation is corroborated by numerical simulations. When the field is further increased, we find that the droplet eventually collapses under the pressure from the Zeeman energy. © *2014 AIP Publishing LLC*. [http://dx.doi.org/10.1063/1.4870696]

I. INTRODUCTION

A. Spin torque oscillators

Spin transfer torque (STT)[1–3] is a dissipative phenomenon in which a spin-polarized current transfers angular momentum to the local magnetization and directly impacts its magnetodynamics. Depending on the details of the magnetic state, and of the sign of the spin-polarized current, STT can either increase or decrease the local damping. The damping can be decreased to such an extent that even negative spin wave (SW) damping (i.e., gain) can be realized locally. Negative (linear) damping is the basis for the so-called spin torque oscillator (STO), in which a steady state of very high amplitude SWs can be sustained indefinitely when STT is balanced by additional non-linear damping processes.[4–7] STOs are typically fabricated in one of two principally different architectures: (i) Nano-pillars, where the lateral cross section of the entire device has been reduced to a typically <100 nm diameter,[8] and (ii) nano-contacts (NC),[9] where only the current injection site has been laterally confined and the current enters, and spreads out into, a much larger magnetic area. The magnetically active part of the device typically consists of a ferromagnet/spacer/ferromagnet trilayer, where one of the ferromagnetic (FM) layers is fixed, either via pinning to adjacent magnetic layers or by virtue of being thicker, and the other FM layer is free to host a high intensity of SW excitations. In nano-pillars, the spacer can either be metallic, as in pseudo spin valves (PSVs), or insulating, as in magnetic tunnel junctions (MTJs). In the former, the final microwave signal is generated via the giant magnetoresistance (GMR) in the PSV; in the latter, a significantly larger microwave signal can be generated through the much higher tunneling magnetoresistance (TMR).[10–12] Nano-contact STOs (NC-STOs), on the other hand, are almost entirely based on PSVs. Very recently, single-layer NC-STOs have also been reported, where a single FM layer gets excited by STT resulting from an asymmetric spin accumulation at each interface to a non-magnetic metal and the microwave signal is generated via the anisotropic magnetoresistance (AMR).[13]

STOs are fundamentally interesting since their microwave signals result from the interplay between spin-dependent transport through magnetic heterostructures, strongly nonlinear magnetization processes, and SW modes in nanomagnets. The strong nonlinearity and the large number of fundamentally different SW modes lead to a wide range of available microwave frequencies and many different current and field dependences to control those signals. From an applied perspective, STOs offer the prospect of extremely frequency-tunable[14,15] and rapidly modulated[16–24] microwave generators on the nanoscale, with potential applications in mobile telecommunications, vehicle radar, and microwave spectroscopy.[25,26]

a)Author to whom correspondence should be addressed. Electronic mail: johan.akerman@physics.gu.se.

Two significant drawbacks still limit the applicability of STOs to primarily fundamental studies of STT and magnetodynamic phenomena; (i) low signal-to-noise ratio (SNR) stemming from a limited output power and high phase noise and (ii) magnetic field requirements. The SNR can be improved by increasing the output power and increasing the STO signal coherence. While the highest output power is achieved in MTJ based STOs,[10–12] their multi-modal nature severely limits their coherence.[27–29] NC-STOs still show the highest coherence, which can be further improved using SW mediated synchronization.[30–32] The magnetic droplet soliton discussed in this work demonstrates yet another approach in that the microwave output power increases 40 times, thanks to the much higher SW intensity and more effective use of the available GMR. The drawback of requiring high magnetic fields has been addressed by realizing STOs that combine materials with in-plane (IP) and out-of-plane (OOP) anisotropies.[33–39] As shown in this work, the nucleation of a droplet with significant output power requires a tilted fixed layer magnetization. While this is here achieved by tilting an IP Co fixed layer OOP using strong OOP fields, a zero-field solution should be possible to realize using intrinsically tilted fixed layers.[40–44]

B. The fundamental SW modes in STOs

In nano-pillar STOs, the SW modes are typically directly related to the available linear sub-threshold SW modes given by the pillar dimensions. These are either located in the center of the element (center mode) where the internal field is basically homogeneous or located near the edges of the nano-pillar (edge mode) where the internal field is inhomogeneous. In nano-pillar MTJ-STOs, fixed layer SW modes can also be observed.[27,28] The modes are often coupled due to non-zero damping (both positive and negative).[29] Nano-pillar STOs can also host vortices, which can undergo gyrotropic motion driven by STT.[35,45]

While the SW modes in NC-STOs are independent of the lateral dimension of the magnetic layers, the diameter of the NC serves as the defining dimension and has a direct impact on the fundamental SW modes excitable in this geometry. Slonczewski predicted[4] that a NC on top of a perpendicularly saturated NiFe film should be able to excite radially propagating SWs with a wave number inversely proportional to the NC radius. In addition, a strongly non-linear, self-localized, soliton "bullet" mode can also be excited, provided the magnetization of the NiFe lies significantly more in-plane.[46–53] The intrinsically inhomogeneous nature of the Oersted field in the vicinity of the NC leads to a physical separation of the two modes, and even to strong localization of both SW modes at opposite ends of the NC. Therefore, the size of the NC governs the degree of mode cross-talk leading to intermodulation products, mode-hopping, and mode coexistence behaviors.[54] NC-STOs, consequently, hold great promise for magnonics applications since they can generate short wavelength propagating spin waves,[55,56] which through the Oersted field can even be focused into SW directional beams.[57] The Oersted field can also induce vortex-antivortex pairs, where the vortex can undergo gyrotropic motion in a similar manner as in nano-pillars.[13,58–60]

C. Magnon drops and magnetic droplets

Of particular importance for the present study is the concept of SW solitons in free layers with a perpendicular equilibrium orientation of the magnetization, i.e., with sufficient perpendicular magnetic anisotropy (PMA) to overcome the demagnetization field. As first demonstrated analytically by Ivanov *et al.*,[61,62] the Landau-Lifshitz equation for such magnetic films can sustain a family of so-called magnon drop solitons, provided there is no SW damping. The existence of magnon drop solitons finds its foundation in the semi-quantum mechanical description of magnons (SW quasi-particles) in materials with PMA. The Hamiltonian describing the interaction between magnons, performing the usual Holstein-Primakoff transformation[63] to expand the magnon creation and annihilation operators, acquires an attractive form. In other words, magnons in materials with PMA attract each other and can form a condensate. The increasing density of magnons ultimately leads to instability, i.e., the exponential growth of the SW amplitude, where the magnetically homogeneous state is deformed into a magnon drop, stabilized by the balance between exchange and anisotropy. Consequently, magnon drops are non-topological and are furthermore characterized by a dispersion law that defines a family of possible solutions to the conservative system (Fig. 1).

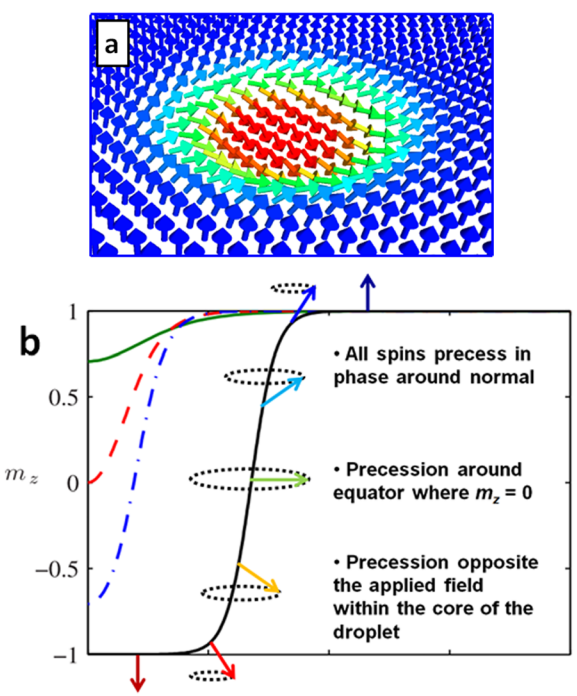

FIG. 1. (a) A 2-dimensional magnetization snapshot of a PMA material where a high density of SWs have locally condensed into a magnon drop. All spins not perfectly aligned with the PMA axis precess around this axis, all with the same frequency but with a radially varying precession angle. The core can be partially or (almost) fully reversed depending on the magnon density in the drop. (b) A radial cross section of the time averaged perpendicular component of the magnetization for four different drops with different magnon densities. The black solid line shows a magnon drop with a very high density where effectively only the spins in the perimeter precess. The arrows indicate the local precession angle, which can approach 180° (almost fully reversed) in the center of the drop. The droplets studied experimentally in this work are best described by a profile in between the dashed red line and the dashed-dotted blue line.

While any metal based magnetic system always exhibits substantial SW damping, hence making magnon drops unrealistic, it was recently argued by Hoefer, Keller, and Silva that NC-STOs should, in principle, be able to emulate a damping-free material in a region underneath the NC where the balance between STT and SW damping provides the necessary (time-averaged) zero net damping condition.[64,65] In their analytical and numerical analysis of such devices, they indeed demonstrated that magnon-drop-like excitations should be possible. In contrast to the conservative magnon drops, these so-called magnetic droplets are strongly dissipative, relying not only on the original balance between exchange and anisotropy but also on the balance between STT and non-linear damping. As a consequence, out of the large family of magnon drops, the additional net zero damping condition singles out a particular magnetic droplet with both a well-defined frequency and a well-defined degree of core reversal.

The final experimental confirmation of magnetic droplet solitons was recently reported in Ref. 66. Here, we describe in detail the nucleation of magnetic droplet solitons as a function of both applied field and current. We also expand our study to magnetic droplets at much higher fields, where we observe clear signatures of droplets collapsing under the pressure of the increasing Zeeman energy.

II. SAMPLE PREPARATION

Orthogonal-pseudo spin valves (Ortho-PSVs) were made from bottom-to-top: Co(6 nm) easy-plane anisotropy as reference layer, Cu(6 nm) spacer, and Co(0.2 nm)-[Ni(0.6 nm)/Co(0.25 nm)]$_4$ ML with PMA as free layer. These stacks were deposited by magnetron sputtering at room temperature on thermally oxidized Si substrates in a chamber with a base pressure lower than 5×10^{-8} Torr. The sputtering growth rate used for the ultra-thin Co and Ni layers was less than 0.2–0.3 Å/s to maximize uniformity and minimize interdiffusion. A Ta(4 nm)/Cu(10 nm)/Ta(4 nm) stack with strong (111)-texture was used as a seed layer to maximize the PMA of the Co/Ni ML and also to act as low resistance bottom electrode for the current path under the NC to minimize lateral current spreading in the STO devices. Finally, the whole stack is capped with Cu(2 nm)/Pd(2 nm) to prevent oxidation. Hysteresis loops of both the magnetoresistance and the magnetization of the unpatterned material stack are shown in Fig. 2. As always for Ortho-PSVs, both the IP and OOP loops exhibit a strongly sheared hard-axis behavior as either the Co fixed layer or the [Co/Ni] free layer is forced away from its easy direction. Using the linear slope of the in-plane magnetoresistance (IP-MR) loop, red open circles in Fig. 2(a), we can extrapolate an approximate saturation field of $\mu_o(H_k - M_S) = 0.35$ T for the [Co/Ni]. From alternating gradient magnetometry (AGM), we estimate the [Co/Ni] saturation magnetization to $\mu_o M_S = 0.95$ T.

Fabrication of the Ortho-NC-STOs includes the following steps: (i) Patterning the blanket films to a $8 \times 16\ \mu m^2$ mesa using optical lithography, (ii) deposition of an insulating SiO_2 layer by chemical vapor deposition, (iii) defining the NC area using electron-beam lithography, (iv) reactive ion etching through the SiO_2 to define the NC, (v) deposition of a top contact electrode of Cu(1.1 μm)/Au(100 nm), and (vi) forming the electrodes into a coplanar waveguide using optical lithography and lift-off.

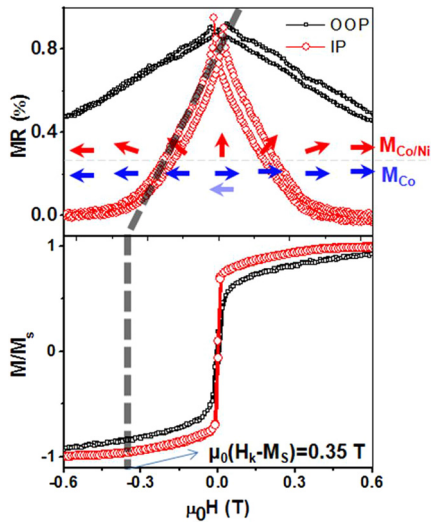

FIG. 2. IP and OOP hysteresis loops of (a) the MR and (b) the magnetization. Inset in (b) is the same plot at higher fields.

A custom probe station was used for electrical characterization of the STO devices under variable current, magnetic field (±2 T), and applied field angle at room temperature. The resulting microwave signal from STO devices was amplified using a broadband microwave amplifier and measured in the frequency domain with a spectrum analyzer. The DC voltage was simultaneously measured across the device for MR measurements.

III. RESULTS AND DISCUSSION

A. Pre-droplet operation

Low-field operation (0.2 T) of an Ortho-NC-STO with a NC diameter of 65 nm is shown in Fig. 3. The measured onset microwave frequency (18 GHz) agrees well with the expected free layer precession frequency[36] given by $f = \gamma\mu_0/2\pi[H + (H_k - M_S)\cos(\theta)]$, where θ is the precession angle of the free layer. The inset shows how the microwave frequency at threshold increases linearly with applied field, as expected for this FMR-like SW mode; two different NC-STOs of nominally the same diameter also show very similar behavior. As the current is increased, the integrated microwave power increases, while the frequency slowly red-shifts. The current induced red-shift is a consequence of the increasing precession angle θ.

B. Droplet nucleation

The behavior of the same device in moderate to high fields is shown in Fig. 4. At a critical field of $\mu_0 H_{droplet} = 0.65$ T, five distinct transitional phenomena can be observed: (i) The precession frequency exhibits a dramatic 10 GHz drop from about 30 GHz to 20 GHz, (ii) the integrated microwave power (P) increases 40 times from 5 pW to a maximum of about 200 pW, (iii) the device resistance exhibits a

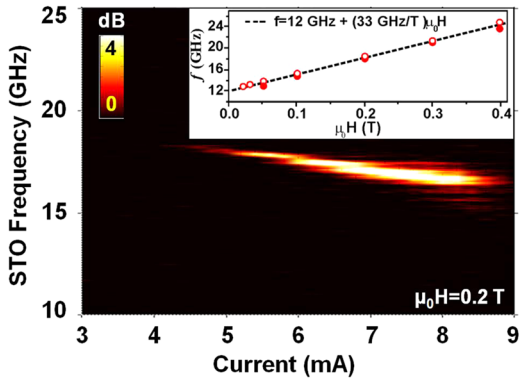

FIG. 3. STO operating frequency versus current in the pre-droplet regime at $\mu_0 H = 0.2$ T. The inset shows the frequency at threshold of two 63 and 65 nm NCs at different fields.

jump, (iv) the magnetoresistance changes sign, and (v) modulation sidebands appear around the main precession frequency. As will be discussed below, all five observations are clear signatures of the nucleation of a magnetic droplet soliton.

The sharp drop in frequency is related to the soliton finding a balance between exchange, anisotropy, STT, and non-linear damping. As explained in detail in Ref. 57, conservative (zero linear damping) magnetic droplet can in principle take on any frequency between the FMR frequency and that given by replacing the effective field with only the applied field (the so-called Zeeman frequency in Ref. 57). Balance between the exchange energy and the anisotropy

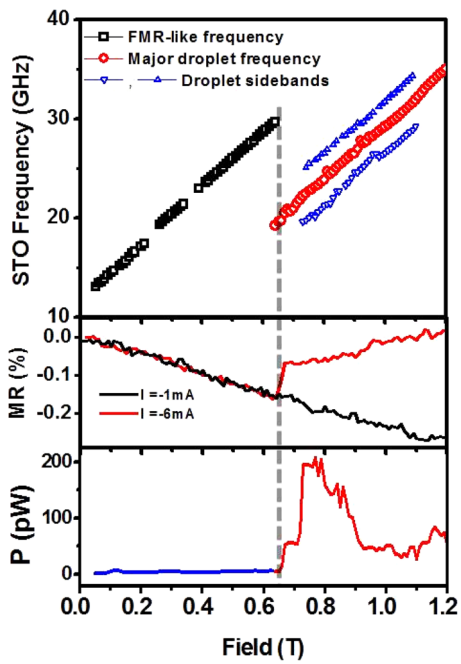

FIG. 4. Frequency, integrated power (P), and MR as a function of perpendicular magnetic field at a constant current of −6 mA through an Ortho-NC-STO with 63 nm NC diameter. Below a droplet nucleation field of about $\mu_0 H_{droplet} = 0.65$ T, the ordinary FMR-like signal is observed, increasing linearly with a 28.7 GHz/T slope. The DC MR shows a linear decrease of −0.25%/T. At $\mu_0 H_{droplet}$ the frequency drops by about 10 GHz and modulation sidebands appear. MR experiences a simultaneous jump by 0.1% and its field dependence changes sign to a positive linear slope of 0.17%/T. The integrated power jumps from 5 pW to 200 pW in two steps.

energy at any such frequency can be a realized by a particular radial profile of the conservative magnetic droplet. Each droplet can be described uniquely by either the degree of core reversal or the reduction in frequency compared to FMR. For example, the four radial profiles depicted in Fig. 1(b) correspond to droplets with approximately 25%, 50%, 80%, and 100% core reversal, and a 6%, 13%, 48%, and 85% reduction of its frequency compared to FMR. In the case of actual and strongly dissipative magnetic droplet solitons, these profiles are only slightly modified.[57] The ~33% reduction in frequency observed in Fig. 4 corresponds to a radial profile in between the dashed red line and the dashed-dotted blue line in Fig. 1(b). From the amount of frequency drop alone, one can hence already predict that the experimentally observed droplet should have a partially reversed core.

The sharp increase in integrated microwave power, of as much as 40 times, provides a further strong indication that a droplet has formed. If the core of the droplet is indeed partially reversed, a large fraction of the droplet will have precession angles close to the equator and hence make much better use of the available GMR of the material stack.

The jump in resistance indicates that the magnetic state has changed into a more antiparallel orientation. As shown in the inset of Fig. 4, the resistance of the device first decreases linearly with field, as expected for a slowly OOP tilting Co fixed layer. As it is highly unlikely that this tilt angle changes abruptly at a certain field, the only plausible explanation is a change in the magnetic state of the free layer. Again, the nucleation of a droplet can directly explain this observation. Furthermore, the sign change of the MR is a direct consequence of the partial reversal of the droplet core. Without the reversal, the MR would still be negative, albeit with a weaker slope. The sign change, and the significant positive MR above the critical field, points to a substantially reversed droplet core.

The final observation, the appearance of equidistant side bands, is not as easily explained by droplet nucleation alone. The sidebands indicate that an additional dynamic phenomenon modulates the original precession frequency. Our micromagnetic simulations show that one such possible phenomenon might be related to the so-called drift instability[57] where, under certain conditions, the droplet can escape the NC and as it leaves the region of strong STT eventually succumbs to the high non-linear and linear damping. By modifying the simulation parameters, it is possible to realize a situation where the droplet never leaves the NC region but instead carries out a periodic translational movement. The resulting instantaneous resistance is shown in Fig. 5(a) and exhibits two very different frequency components, the higher given by the rapid precession of the spins, and the lower associated with the translational motion of the entire droplet. Fig. 5(b) shows a fast Fourier transform of the simulated time trace, clearly demonstrating how the slow dynamical process modulates the main precession frequency and results in equidistant modulation sidebands. The inset in Fig. 5(b) shows snapshots of the free layer magnetization during the simulation. While we find a qualitative agreement with our simulations, the experimentally observed sidebands appear

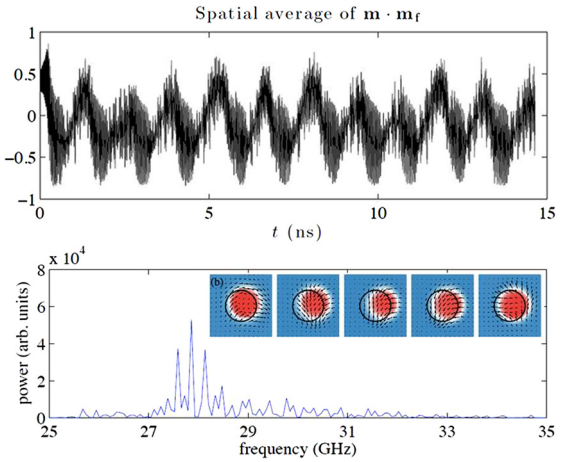

FIG. 5. Micromagnetic simulations of a droplet exhibiting a periodic translational motion. (a) The scalar product of the free and the fixed layer directly underneath the NC showing two very different frequencies, the higher given by the rapid precession of the spins, and the lower associated with the translational motion of the entire droplet. (b) A fast Fourier transform of the time traced in (a). Inset shows snapshots of the free layer magnetization during the simulation.

at about 0.9–1.5 GHz, i.e., at higher frequency than the simulations. Other simulated phenomena, such as droplet spinning,[66] could potentially be excited but do not show any better agreement, since they appear at yet much higher frequency (>5 GHz). Further experimental study, such as direct microscopic droplet observation, is therefore needed to determine exactly which intrinsic droplet phenomenon is responsible for the observed sidebands.

C. Droplet collapse

We finally turn to the high-field droplet regime. In an Ortho-NC-STO the applied OOP field affects the fixed layer and the free layer in different ways, and the net result on the droplet is not trivial. As discussed in Ref. 66, a prerequisite for droplet nucleation is a sufficient perpendicular component of the spin polarized current density. To achieve any perpendicular component of the spin polarization, the fixed layer must be tilted ever so slightly OOP. To reach the critical current density, a sufficient current must then be driven through the NC. The greater the fixed layer tilt angle, the lower the critical current density. As a consequence, the critical current density scales inversely with the applied field.[66] However, this simple relation only holds up until the OOP saturation of the fixed layer, and if the field is further increased, a second effect eventually becomes more important: the Zeeman energy of the droplet itself. The partially reversed volume of magnetization underneath the NC comes at a great cost in Zeeman energy, which grows linearly with the applied field. As long as the perpendicular component of the fixed layer also grows linearly with field, the droplet remains energetically favorable, but once the fixed layer is saturated, the Zeeman energy can in principle dominate.

To test this hypothesis, we measured the NC-STO resistance to very high fields as a probe of whether a droplet is present underneath the NC. Fig. 6 shows the normalized NC-STO resistance for two currents, one below and the

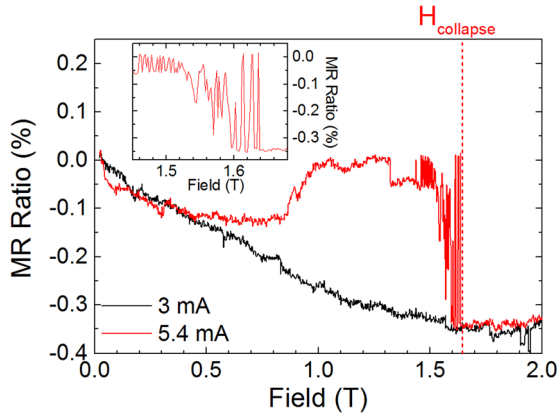

FIG. 6. MR of an Ortho-NC-STO measured below (I = 3 mA; black curve) and above (I = 5.4 mA; red curve) threshold. Above threshold, the droplet is fully formed at about 1 T. As the OOP field is further increased, the droplet becomes unstable and finally collapses at about 1.64 T.

other above the droplet nucleation threshold. Below threshold, the NC-STO resistance first decreases linearly with field to finally saturate at about 1.6 T when the Co fixed layer magnetization saturates OOP. Above threshold, the NC-STO resistance is first identical to below threshold, and then increases at a certain critical field value where the fixed layer tilts enough to provide sufficient STT for droplet nucleation. In this particular device, there are also signs of additional transitions, possibly indicating structural changes in the droplet.[67] However, as the field is further increased, there are clear signs of droplet instabilities and for fields above 1.64 T, both resistance curves again overlap. We interpret this as a collapse of the droplet when the Zeeman energy becomes prohibitively large. The inset in Fig. 6 shows how the NC-STO resistance fluctuates strongly between values consistent with a fully developed droplet and no droplet. In a certain field range, the competition between STT and the Zeeman energy hence seems to allow for these two relatively stable states, possibly indicating thermally driven droplet collapse and rebirth in a region where STT and the Zeeman energy are of similar strength. Time-resolved resistance measurements at constant field would probably shed more light on the time constant for such possible mode hopping. For higher drive currents, increasingly higher fields are required to make the droplet collapse, and the transition becomes entirely sharp and non-fluctuating.

IV. CONCLUSIONS

Nano-contact spin torque oscillators were fabricated using orthogonal pseudo spin valves based on Co fixed layers and [Co/Ni] free layers with strong perpendicular magnetic anisotropy. The resistance, magnetoresistance, and microwave properties of these devices were studied as a function of current and out-of-plane magnetic field. At low fields, the NC-STOs show a FMR-like behavior. At intermediate fields, a dramatic transition to a magnetic droplet state can be observed at a critical field. The NC-STO resistance, magnetoresistance, and microwave signal all indicated the nucleation of a magnetic droplet soliton. At very high fields, where

the fixed layer is saturated out-of-plane, the droplets are eventually found to collapse under the pressure from the Zeeman energy.

ACKNOWLEDGMENTS

This work was supported by the EC FP7 Contract No. ICT-257159 "MACALO," the Swedish Foundation for Strategic Research (SSF), the Swedish Research Council (VR), and the Knut and Alice Wallenberg Foundation. Johan Åkerman is a Royal Swedish Academy of Sciences Research Fellow supported by a grant from the Knut and Alice Wallenberg Foundation.

[1]L. Berger, Phys. Rev. B **54**, 9353 (1996).
[2]J. Slonczewski, J. Magn. Magn. Mater. **159**, L1 (1996).
[3]D. Ralph and M. Stiles, J. Magn. Magn. Mater. **320**, 1190 (2008).
[4]J. C. Slonczewski, J. Magn. Magn. Mater. **195**, L261 (1999).
[5]T. Silva and W. Rippard, J. Magn. Magn. Mater. **320**, 1260 (2008).
[6]A. Slavin and V. Tiberkevich, IEEE Trans. Magn. **45**, 1875 (2009).
[7]J.-V. Kim, Solid State Phys. **63**, 217 (2012).
[8]S. I. Kiselev, J. C. Sankey, I. N. Krivorotov, N. C. Emley, R. J. Schoelkopf, R. A. Buhrman, and D. C. Ralph, Nature **425**, 380 (2003).
[9]M. Tsoi, A. G. M. Jansen, J. Bass, W.-C. Chiang, M. Seck, V. Tsoi, and P. Wyder, Phys. Rev. Lett. **80**, 4281 (1998); Nature **406**, 46 (2000).
[10]A. V. Nazarov, K. Nikolaev, Z. Gao, H. Cho, and D. Song, J. Appl. Phys. **103**, 07A503 (2008).
[11]A. M. Deac, A. Fukushima, H. Kubota, H. Maehara, Y. Suzuki, S. Yuasa, Y. Nagamine, K. Tsunekawa, D. D. Djayaprawira, and N. Watanabe, Nat. Phys. **4**, 803 (2008).
[12]D. Houssameddine, S. H. Florez, J. A. Katine, J.-P. Michel, U. Ebels, D. Mauri, O. Ozatay, B. Delaet, B. Viala, L. Folks, B. D. Terris, and M.-C. Cyrille, Appl. Phys. Lett. **93**, 022505 (2008).
[13]S. R. Sani, P. Dürrenfeld, S. M. Mohseni, S. Chung, and J. Åkerman, IEEE Trans. Magn. **49**, 4331 (2013).
[14]W. H. Rippard, M. R. Pufall, S. Kaka, T. J. Silva, and S. E. Russek, Phys. Rev. B **70**, 100406(R) (2004).
[15]S. Bonetti, P. Muduli, F. Mancoff, and J. Åkerman, Appl. Phys. Lett. **94**, 102507 (2009).
[16]M. R. Pufall, W. H. Rippard, S. Kaka, T. J. Silva, and S. E. Russek, Appl. Phys. Lett. **86**, 082506 (2005).
[17]P. K. Muduli, Y. Pogoryelov, S. Bonetti, G. Consolo, F. Mancoff, and J. Åkerman, Phys. Rev. B **81**, 140408(R) (2010).
[18]G. Consolo, V. Puliafito, G. Finocchio, L. Lopez Diaz, R. Zivieri, L. Giovannini, F. Nizzoli, G. Valenti, and B. Azzerboni, IEEE Trans. Magn. **46**, 3629 (2010).
[19]P. K. Muduli, Y. Pogoryelov, F. Mancoff, and J. Åkerman, IEEE Trans. Magn. **47**, 1575 (2011).
[20]P. K. Muduli, Y. Pogoryelov, Y. Zhou, F. Mancoff, and J. Åkerman, Integr. Ferroelectr. **125**, 147 (2011).
[21]Y. Pogoryelov, P. K. Muduli, S. Bonetti, E. Iacocca, F. Mancoff, and J. Åkerman, Appl. Phys. Lett. **98**, 192501 (2011).
[22]Y. Pogoryelov, P. K. Muduli, S. Bonetti, F. Mancoff, and J. Åkerman, Appl. Phys. Lett. **98**, 192506 (2011).
[23]E. Iacocca and J. Åkerman, Phys. Rev. B **85**, 184420 (2012).
[24]Ye. Pogoryelov, P. K. Muduli, and J. Åkerman, IEEE Trans. Magn. **48**, 4077 (2012).
[25]P. Villard, U. Ebels, D. Houssameddine, J. Katine, D. Mauri, B. Delaet, P. Vincent, M.-C. Cyrille, B. Viala, J.-P. Michel, J. Prouvee, and F. Badets, IEEE J. Solid-State Circuits **45**, 214 (2010).
[26]J. Persson, S. R. Sani, S. Bonetti, F. Magnusson, Ye. Pogoryelov, S. M. Mohseni, S. Gunnarsson, M. Norling, C. Stoij, and J. Åkerman, IEEE Trans. Magn. **48**, 4378 (2012).
[27]A. Helmer, S. Cornelissen, T. Devolder, J.-V. Kim, W. van Roy, L. Lagae, and C. Chappert, Phys. Rev. B **81**, 094416 (2010).
[28]P. K. Muduli, O. H. Heinonen, and J. Åkerman, Phys. Rev. B **83**, 184410 (2011).
[29]P. K. Muduli, O. G. Heinonen, and J. Åkerman, Phys. Rev. Lett. **108**, 207203 (2012).
[30]F. B. Mancoff, N. D. Rizzo, B. N. Engel, and S. Tehrani, Nature **437**, 393 (2005).
[31]S. Kaka, M. R. Pufall, W. H. Rippard, T. J. Silva, S. E. Russek, and J. A. Katine, Nature **437**, 389 (2005).
[32]S. R. Sani, J. Persson, M. S. Mohseni, Ye. Pogoryelov, P. K. Muduli, A. Eklund, G. Malm, M. Käll, A. Dmitriev, and J. Åkerman, Nat. Commun. **4**, 2731 (2014).
[33]T. Devolder, A. Meftah, K. Ito, J. A. Katine, P. Crozat, and C. Chappert, J. Appl. Phys. **101**, 063916 (2007).
[34]D. Houssameddine, U. Ebels, B. Delaët, B. Rodmacq, I. Firastrau, F. Ponthenier, M. Brunet, C. Thirion, J.-P. Michel, L. Prejbeanu-Buda, M.-C. Cyrille, O. Redon, and B. Dieny, Nature Mater. **6**, 447 (2007).
[35]V. S. Pribiag, I. N. Krivorotov, G. D. Fuchs, P. M. Braganca, O. Ozatay, J. C. Sankey, D. C. Ralph, and R. A. Buhrman, Nat. Phys. **3**, 498 (2007).
[36]W. H. Rippard, A. M. Deac, M. R. Pufall, J. M. Shaw, M. W. Keller, S. E. Russek, and C. Serpico, Phys. Rev. B **81**, 014426 (2010).
[37]S. M. Mohseni, S. R. Sani, J. Persson, T. N. Anh Nguyen, S. Chung, Ye. Pogoryelov, and J. Åkerman, Phys. Status Solidi - Rapid Res. Lett. **5**, 432–434 (2011).
[38]Y. Zhou, C. L. Zha, S. Bonetti, J. Persson, and J. Åkerman, Appl. Phys. Lett. **92**, 262508 (2008).
[39]Y. Zhou, S. Bonetti, C. L. Zha, and J. Åkerman, New J. Phys. **11**, 103028 (2009).
[40]C. L. Zha, J. Persson, S. Bonetti, Y. Fang, and J. Åkerman, Appl. Phys. Lett. **94**, 163108 (2009).
[41]T. N. Anh Nguyen, Y. Fang, V. Fallahi, N. Benatmane, S. M. Mohseni, R. K. Dumas, and J. Åkerman, Appl. Phys. Lett. **98**, 172502 (2011).
[42]T. N. Anh Nguyen, N. Benatmane, V. Fallahi, Y. Fang, S. M. Mohseni, R. K. Dumas, and J. Åkerman, J. Magn. Magn. Mater. **324**, 3929 (2012).
[43]S. Chung, S. M. Mohseni, V. Fallahi, T. N. Anh Nguyen, N. Benatmane, R. K. Dumas, and J. Åkerman, J. Phys. D: Appl. Phys. **46**, 125004 (2013).
[44]S. Tacchi, T. N. Anh Nguyen, G. Carlotti, G. Gubbiotti, M. Madami, R. K. Dumas, J. W. Lau, J. Åkerman, A. Rettori, and M. G. Pini, Phys. Rev. B **87**, 144426 (2013).
[45]S. Kasai, Y. Nakatani, K. Kobayashi, H. Kohno, and T. Ono, Phys. Rev. Lett. **97**, 107204 (2006).
[46]A. Slavin and V. Tiberkevich, Phys. Rev. Lett. **95**, 237201 (2005).
[47]W. H. Rippard, M. R. Pufall, and T. J. Silva, Appl. Phys. Lett. **82**, 1260 (2003).
[48]G. Consolo, B. Azzerboni, G. Gerhart, G. A. Melkov, V. Tiberkevich, and A. N. Slavin, Phys. Rev. B **76**, 144410 (2007).
[49]D. V. Berkov and N. L. Gorn, Phys. Rev. B **76**, 144414 (2007).
[50]G. Consolo, B. Azzerboni, L. Lopez-Diaz, G. Gerhart, E. Bankowski, V. Tiberkevich, and A. N. Slavin, Phys. Rev. B **78**, 014420 (2008).
[51]D. Berkov and J. Miltat, J. Magn. Magn. Mater. **320**, 1238 (2008).
[52]S. Bonetti, V. Tiberkevich, G. Consolo, G. Finocchio, P. Muduli, F. Mancoff, A. Slavin, and J. Åkerman, Phys. Rev. Lett. **105**, 217204 (2010).
[53]S. Bonetti, V. Puliafito, G. Consolo, V. S. Tiberkevich, A. N. Slavin, and J. Åkerman, Phys. Rev. B **85**, 174427 (2012).
[54]R. K. Dumas, E. Iacocca, S. Bonetti, S. R. Sani, S. M. Mohseni, A. Eklund, J. Persson, O. Heinonen, and J. Åkerman, Phys. Rev. Lett. **110**, 257202 (2013).
[55]M. Madami, S. Bonetti, G. Consolo, S. Tacchi, G. Carlotti, G. Gubbiotti, F. B. Mancoff, M. A. Yar, and J. Åkerman, Nat. Nanotechnol. **6**, 635 (2011).
[56]H. Ulrichs, V. E. Demidov, S. O. Demokritov, and S. Urazhdin, Appl. Phys. Lett. **100**, 162406 (2012).
[57]M. A. Hoefer, T. J. Silva, and M. D. Stiles, Phys. Rev. B **77**, 144401 (2008).
[58]M. Pufall, W. Rippard, M. Schneider, and S. Russek, Phys. Rev. B **75**, 140404 (2007).
[59]Q. Mistral, M. van Kampen, G. Hrkac, J.-V. Kim, T. Devolder, P. Crozat, C. Chappert, L. Lagae, and T. Schrefl, Phys. Rev. Lett. **100**, 257201 (2008).
[60]D. V. Berkov and N. L. Gorn, Phys. Rev. B **80**, 064409 (2009).
[61]B. A. Ivanov and A. M. Kosevich, Zh. Eksp. Teor. Fiz. **72**, 2000 (1977) [Sov. Phys. JETP **45**, 1050 (1977)].
[62]A. M. Kosevich, B. A. Ivanov, and A. S. Kovalev, Phys. Rep. **194**, 117 (1990).
[63]T. Holstein and H. Primakoff, Phys. Rev. **58**, 1098 (1940).
[64]M. Hoefer, T. Silva, and M. Keller, Phys. Rev. B **82**, 054432 (2010).
[65]M. Hoefer, M. Sommacal, and T. Silva, Phys. Rev. B **85**, 214433 (2012).
[66]S. M. Mohseni, S. R. Sani, J. Persson, T. N. A. Nguyen, S. Chung, Y. Pogoryelov, P. K. Muduli, E. Iacocca, A. Eklund, R. K. Dumas, S. Bonetti, A. Deac, M. A. Hoefer, and J. Åkerman, Science **339**, 1295 (2013).
[67]S. M. Mohseni, S. R. Sani, R. K. Dumas, J. Persson, T. N. Anh Nguyen, S. Chung, Ye. Pogoryelov, P. K. Muduli, E. Iacocca, A. Eklund, and J. Åkerman, Phys. B Condens. Matter **435**, 84 (2014).